JOURNAL OF GUIDANCE, CONTROL, AND DYNAMICS
Vol. 21, No. 4, July–August 1998

Pulse Motor Optimization via Mission Charts for an Exoatmospheric Interceptor

Craig A. Phillips* and D. Stephen Malyevac†
U.S. Naval Surface Warfare Center, Dahlgren, Virginia 22448

The selection of the pulse split and the interpulse delay of a two-pulse exoatmospheric midcourse stage for an exoatmospheric interceptor, which uses a kinetic kill vehicle (KKV) for a direct hit kill, is examined. Mission chart analysis is introduced along with system error trees and is used to select motor parameters that maximize the complete weapon system performance. In this analysis, the interceptor receives measured target updates from a weapon system consisting of a track sensor and a link to the interceptor. Location of the weapon system track sensor is not restricted by this analysis. The interceptor states may be measured by the interceptor, by the weapon system track sensor, or by some combination of these. For specific weapon system and interceptor errors, the mission charts indicate upper and lower limits on the second-pulse burnout time. Ignition of the second pulse anywhere between these bounds leads to a high probability of a successful intercept with the earliest ignition time generally producing the highest average speed. These bounds are a function of 1) the KKV divert capability, 2) the weapon system and interceptor errors, 3) the fraction of second-pulse impulse allotted for midcourse correction divert, and 4) the propellant split between the first and second pulse. As the total mission time to intercept increases, the difference between the upper and lower bounds decreases until the mission becomes infeasible. The system errors and the pulse split determine the maximum feasible mission time. For a specific set of errors, there is a pulse split that optimizes the maximum feasible mission time and intercept range when all system constraints are considered. The maximum feasible intercept range is extremely sensitive to the system errors.

Nomenclature

K_{ge} = guidance efficiency of the kinetic kill vehicle
R_{go} = range-to-go to the intercept point, m
t_g = time-to-go to the intercept, s
t_{gmc} = time-to-go to the intercept at the midcourse-stage motor burnout (second pulse), s
$t_{gmc\,max}$ = maximum allowable time-to-go to the intercept of the midcourse-stage motor burnout (second pulse), s
$t_{gmc\,min}$ = minimum allowable time-to-go to the intercept of the midcourse-stage motor burnout (second pulse), s
t_{g1bo} = time-to-go to the intercept of the first-pulse burnout of the midcourse stage, s
t_{KKV} = total homing time of the kinetic kill vehicle, s
$t_{mission}$ = total flight time from launch to the intercept, s
t_{p1bo} = flight time at burnout of first pulse, s
t_1 = nominal burn time of the first pulse of the midcourse stage, s
t_2 = nominal burn time of the second pulse of the midcourse stage, s
t_{2ignt} = ignition time of the midcourse-stage second pulse, s
V_{MR1} = average speed remaining to intercept at midcourse-stage first-pulse burnout, m/s
V_{MR2} = average speed remaining to intercept at midcourse-stage second-pulse burnout, m/s
ZEM_{HE} = zero effort miss due to interceptor attitude measurement and control error, m
ZEM_{HEC} = zero effort miss due to errors in interceptor attitude control, m
ZEM_{HEN} = zero effort miss due to interceptor attitude measurement error, m
ZEM_{MPOS} = zero effort miss due to the interceptor position measurement error, m
ZEM_{POS} = zero effort miss due to the combined position measurement errors for the interceptor and the target, m
ZEM_{PTGT} = zero effort miss due to target position measurement error, m
ZEM_{VTGT} = zero effort miss due to target velocity measurement error, m
ZEM_3 = total zero effort miss at midcourse-stage burnout, m
ZEM_{31} = total zero effort miss at midcourse-stage first-pulse burnout, m
Δ_{KKV} = total potential lateral divert displacement of kinetic kill vehicle, m
ΔV_{KKV} = total potential lateral divert velocity of kinetic kill vehicle, m/s
ΔV_{2PUL} = total lateral divert velocity of second pulse allowed for lateral maneuver, m/s
Δ_{2PUL} = total lateral divert displacement of second pulse allowed for lateral maneuver, m
ρ = correlation coefficient between quantities
σ^2_{HE} = variance of the total interceptor attitude measurement and control error, rad^2
σ^2_{HEC} = variance of the total interceptor attitude control error, rad^2
σ^2_{HEN} = variance of the total interceptor attitude measurement error, rad^2
σ^2_{MPOS} = variance of the interceptor position measurement error, m^2
σ^2_{POS} = variance of the combined interceptor and target position measurement error, m^2
σ^2_{PTGT} = variance of the target position measurement error, m^2
σ^2_{VTGT} = variance of the target velocity measurement error, m^2/s^2
σ^2_{x+y} = variance of the combination of two quantities at an error tree junction

Received July 9, 1997; presented as Paper 97-3687 at the AIAA Guidance, Navigation, and Control Conference, New Orleans, LA, Aug. 11–13, 1997; revision received Jan. 17, 1998; accepted for publication Jan. 17, 1998.

*Senior Domain Engineering Expert, Missile Systems Engineering Branch, Weapons Systems Department, Dahlgren Division, G23, 17320 Dahlgren Road. Senior Member AIAA.

†Senior Domain Engineering Expert, Missile Systems Engineering Branch, Weapons Systems Department, Dahlgren Division, G23, 17320 Dahlgren Road. Member AIAA.

σ_x^2 = variance of an arbitrary quantity at an error tree junction

σ_y^2 = variance of an arbitrary quantity at an error tree junction

Introduction

THE development of practical designs for pulsed solid rocket motors during the 1980s has opened new avenues for the control of missile trajectories. Previously, work has concentrated on missions that remain in the atmosphere where pulse motors have shown benefits for the air-to-air intercept but less promise for the surface-to-air intercept mission. The application of pulse motors for endoatmospheric intercepts has concentrated on energy and flight time management. Through proper design of the motor and control algorithms, the pulsed rocket motor is able to approach the theoretical limits for endoatmospheric missions. Reduced-order optimal control has been used with success to determine pulse ignition laws to minimize time of flight and to maximize final speed during horizontal flight[1–3] of an air-to-air missile. The problem of ignition of the second pulse and trajectory shaping in the vertical plane to minimize the time of flight has been addressed by reduced-order approximations for an air-to-air missile[4] and for a surface-to-surface missile.[2] Parameter optimization has been used to determine the range maximal motor parameters and open-loop trajectory shaping of a two-pulse air-to-surface missile[5] and the optimal parameters for two- and three-pulse surface-to-air missiles.[6] A heuristic two-pulse approximation to the optimal control solution for the thrust and the trajectory shaping for a surface-to-air missile has been presented.[7]

The recent interest in surface launched antitactical ballistic missile interceptors with solid propulsion and using extended exoatmospheric mission segments creates an opportunity for a very useful application of pulse motor technology. The pulse motor design and operation are not used to control the aerodynamic drag impulse as seen in endoatmospheric optimization, but are used to provide midcourse divert during these long midcourse phases so as to place the final kinetic kill vehicle (KKV) inside its handover basket. Here the pulse motor of the exoatmospheric midcourse stage is the only source of divert available to steer out the interceptor and weapon system errors. Allocation of the propellant between the pulses and the ignition of the second pulse for this exoatmospheric operation is a very different problem than has previously been considered.

This paper presents the use of mission charts to optimize the pulse split and interpulse delay for the pulse motor of an exoatmospheric midcourse stage. The mission chart concept is grounded on the error tree model of the weapon system sensor errors, interceptor sensor errors, and interceptor control accuracy. First a notional interceptor missile and a typical antitactical ballistic missile system will be presented. Development of the relationships for the earliest and the latest time-to-go to intercept for burnout of the second pulse of the exoatmospheric midcourse stage will be presented. Finally, numerical results for a notional interceptor will be presented using the mission chart approach to show how system errors influence the optimal pulse motor parameters.

This paper looks at only a subset of possible airframe design trades. Here, the allocation of volume to the KKV and its characteristics are considered fixed. Expansion of trade studies to include the KKV characteristics will result in varying optimal midcourse-stage pulse split values for each KKV/carrier missile definition. Although not included in the present work, the method may be extended to the problem of optimizing the motor design for missions requiring discrimination and divert between a set of target-like objects.

Notional Interceptor and Mission Profile

A notional surface-to-exoatmospheric antitactical ballistic missile interceptor is considered. It consists of three solid propulsion stages with a fourth stage consisting of a KKV. The first two stages operate during the initial endoatmospheric phase and are followed by a two-pulse midcourse-stage after exiting the atmosphere. The KKV then homes on the target using a solid propellant divert system.

The mission sequence for this notional interceptor is shown in Fig. 1. The endoatmospheric guidance for the first two stages flies the interceptor from a vertical launch to a commanded injection

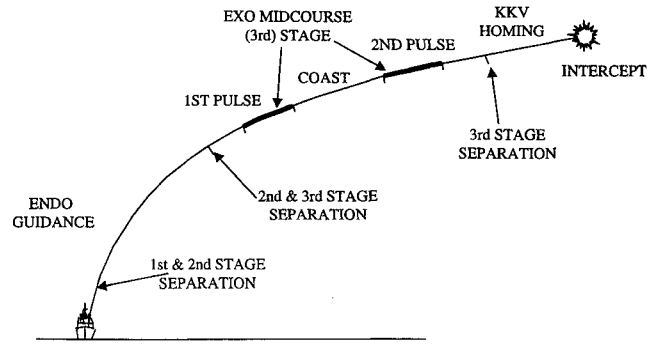

Fig. 1 Exoatmospheric mission profile.

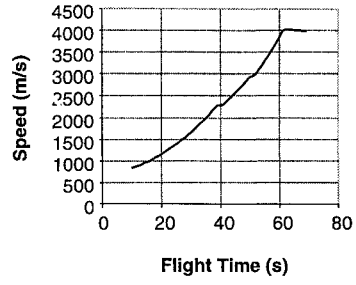

Fig. 2 Notional missile speed history.

vector so that the interceptor is nominally on a course that will allow it to intercept the target with no further steering corrections.

As the interceptor ascends and the dynamic pressure drops, the missile can no longer maintain aerodynamic control and the exoatmospheric midcourse stage separates. This stage is designed to support long exoatmospheric missions and includes a kick motor for increasing the interceptor specific energy and for steering corrections during its burn. The action time of the solid propulsion kick motor is short compared to the length of the exoatmospheric phases for many missions. In this analysis, this motor consists of two pulses. The first pulse is fired early so as to boost the average speed to intercept while correcting the known heading errors from the endoatmospheric phase. The second pulse is then ignited after some interpulse delay and steers out the residual errors from the first pulse. During the motor operation, the midcourse stage uses thrust vector control to point the vehicle centerline and, consequently, the thrust so that heading errors may be corrected. The steering correction on this stage is referred to as a blind divert because it would be conducted without the use of an onboard seeker.

Finally, a solid propulsion KKV would be deployed that acquires the target using a terminal seeker and corrects the residual errors from the midcourse-stage burnout. This vehicle must carry solid propellant to allow a final steering correction, and as such its divert capability is limited. The homing time of the KKV and the divert velocity set the amount of zero effort miss that it may correct. This limit sets the handover basket to which the midcourse stage must deliver the vehicle.

During a mission, each of the exoatmospheric propulsion phases must steer out the residual errors from the previous phase. The inability of any phase to completely steer out the 3σ errors from the previous phase is considered a failed mission design. Thus, both the system errors and the divert of each propulsion phase must be considered in determining a firing window for the second pulse.

Two variants of this notional interceptor are considered in this analysis. These two configurations are similar except for the pulse split of the exoatmospheric midcourse stage. One variant employs a 50/50 propellant pulse split and the other uses an 80/20 split. Table 1 presents some important parameters of these notional interceptor configurations. Figure 2 shows the speed history after second-stage ignition for a specified 1-s interpulse delay for the 50/50-pulse split midcourse-stage pulse motor.

The necessity of many guidance algorithms and of weapons system fire control algorithms to extrapolate interceptor states may require that the amount of trajectory turn and potential forward

Table 1 Interceptor parameters

Parameter	Value
Second-stage initial weight	856 kg
Third- (midcourse-) stage initial weight	265 kg
Third- (midcourse-) stage final weight	131 kg
Third- (midcourse-) stage specific impulse	270 s
KKV potential divert velocity	205 m/s
KKV potential divert displacement	4.6 km
KKV homing time	30 s (nominal) 20 s (minimum)
Midcourse-stage maximum burn angle	25 deg
Second-pulse burnout maximum speed	4 km/s
80/20 first-pulse burnout speed	3.5 km/s
50/50 first-pulse burnout speed	2.9 km/s
Total ΔV of second-pulse for 50/50-pulse split	1.11 km/s
Total ΔV of second-pulse for 80/20-pulse split	0.50 km/s
Allowed lateral divert of second pulse for 50/50	0.47 km/s
Allowed lateral divert of second pulse for 80/20	0.21 km/s
Pulse 1 burnout time	49 s
Pulse 1 and pulse 2 burn time (each)	10 s
KKV guidance efficiency	0.95

velocity variation during the midcourse-stage burn to be limited. Neglecting the relatively small initial transient movement of the thrust vector control nozzle, this forward speed variation may be controlled by limiting the maximum angle between the commanded thrust vector and the velocity vector. This angle is defined as the burn angle.

The burn angle is limited to 25.0 deg, which restricts the available lateral divert of the second pulse. For the 50/50 interceptor, the second pulse can provide a total ΔV of 1110 m/s from Table 1. Under the 25-deg burn angle limit, the lateral divert from the second pulse can be no greater than $1110 \sin(25) = 470$ m/s.

Similarly, the value of 210 m/s of lateral divert for the second pulse of the interceptor with the 80/20 midcourse-stage motor can be computed and is presented in Table 1.

The KKV divert is a function of the inert weight of the KKV, the KKV divert propellant total impulse, the homing time of the KKV, and the divert burn policy of the KKV. This study assumed a KKV with a relatively low mass fraction. The resulting divert velocity is given in Table 1. The solid propellant divert unit has an action time of 30 s so that the KKV is not capable of a blind divert before acquisition of the target by the seeker. The KKV divert propellant grain is assumed to consist of an initial high-rate burn pulse and a lower rate sustain burn pulse, which starts concurrently with the high-rate pulse. If the high-rate burn pulse is assumed to burn instantaneously and the sustain pulse burn occurs over the full KKV homing time with half of the total divert velocity assigned to each pulse, then the divert displacement is given by

$$\Delta_{\mathrm{KKV}} = 0.75 t_{\mathrm{KKV}} \Delta V_{\mathrm{KKV}}$$

Description of the Error Tree Methodology

The error sources contributing to the zero effort miss (ZEM) are grouped into two broad classes consisting of the target tracking errors and the interceptor navigation and control errors. The major error sources modeled on the interceptor side include the attitude measurement error, the interceptor position measurement error, and the guidance and control error. The dominant target track errors include residual weapon system position and velocity measurement errors. To effectively work with these various error sources, a conceptual framework is required. One such approach is the use of an error tree, where each branch associates the ZEM at the intercept with each error source. An important concept is that the ZEM is measured by projecting the trajectory along the heading error in the interceptor velocity from the current time until the intercept. Thus, in the absence of gravitational disturbances or steering corrections, the ZEM, once measured at specific time or mission event, remains fixed.

The error tree represents a particular event and time. Two trees will be constructed. One represents the ZEM at burnout of the second pulse of the midcourse stage. The other is defined at the burnout of the first pulse of the midcourse stage.

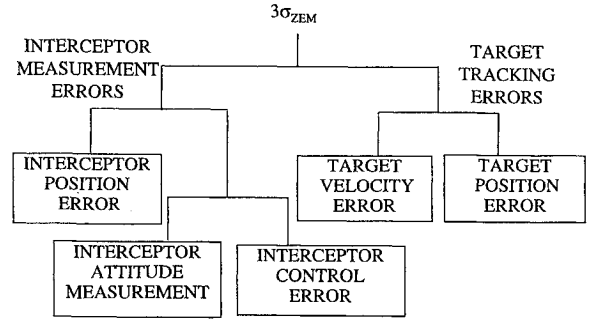

Fig. 3 ZEM error tree.

The error sources may be combined conceptually by means of a series of junction operations as shown in the ZEM tree of Fig. 3. Before combination, each element of the tree is related to the ZEM through the appropriate transformation. The error tree shown in Fig. 3 is appropriate for an application where the missile navigation solution and the target tracking solution are maintained independently. Should the target tracking and the interceptor navigation solution be combined, then the error tree topology will change considerably with some elements disappearing and new ones appearing.

An important aspect of the error tree method is the junction operator, which combines the variances at a junction of the tree. If the correlation between two elements at a junction is known, then the resulting combined variance is given by

$$\sigma_{x+y}^2 = \sigma_x^2 + 2\rho\sigma_x\sigma_y + \sigma_y^2$$

The correlation values may be estimated for each pair of elements at a junction. Typical practice assumes that the elements at each junction are uncorrelated because little correlation information is available for a system under design. If all of the elements are assumed to be uncorrelated, then the topology of the tree may be rearranged for convenience. But if correlation is assumed at any junction, then the tree may not be reconfigured arbitrarily and its topology must be considered very carefully.

The weapon system residual errors include both a target position and a target velocity measurement error after the system estimation and filtering process. For an exoatmospheric phase of a tactical ballistic missile, the accuracy of available gravity models makes the unmodeled target accelerations extremely small so that bias errors may be neglected. The variance of the position error at a given time then translates directly into a variance of the ZEM. The error in the target velocity measurement error is transformed through the current time-to-go to intercept

$$1\sigma\ \mathrm{ZEM}_{\mathrm{PTGT}} = \sigma_{\mathrm{PTGT}}, \qquad 1\sigma\ \mathrm{ZEM}_{\mathrm{VTGT}} = \sigma_{\mathrm{VTGT}} t_g$$

The errors arising from the interceptor navigation and control can be grouped as interceptor direct position measurement error, the interceptor attitude measurement error, and the interceptor guidance and control accuracy. The interceptor direct position error arises from an inertial navigation system (INS), an INS aided by a global positioning system receiver, an INS aided by a weapon system track of the interceptor, or from a direct track of the interceptor in a command guided system. Typically, steady-state error values from an analysis such as presented in Ref. 8 are used. The interceptor navigation position error translates directly into ZEM,

$$1\sigma\ \mathrm{ZEM}_{\mathrm{MPOS}} = \sigma_{\mathrm{MPOS}}$$

The direct position measurement error of the interceptor and of the target may be combined for convenience as long as no correlation is assumed in the error tree:

$$1\sigma\ \mathrm{ZEM}_{\mathrm{POS}} = \sigma_{\mathrm{POS}} = \left(\sigma_{\mathrm{MPOS}}^2 + \sigma_{\mathrm{PTGT}}^2\right)^{\frac{1}{2}}$$

For an INS, the direct velocity magnitude error is typically negligible yet the errors in the transformation from the missile navigation

Table 2 Candidate error sets (3σ values)

Type	Low quality	High quality
Target velocity	52.5 m/s	30 m/s
Target position	440 m	250 m
Missile attitude	11.4 mrad	6.5 mrad
Missile pointing	11.4 mrad	6.5 mrad
Missile position	175 m	100 m

frame and the targeting frame lead to a heading error, which projects through the range-to-go to intercept to yield a ZEM,

$$1\sigma\ \mathrm{ZEM}_{\mathrm{HE}N} = \sigma_{\mathrm{HE}N} R_{\mathrm{go}}$$

Finally, even given perfect navigation information, the exoatmospheric midcourse stage can only compute the guidance solution and control the direction of the velocity vector at burnout to within a finite accuracy. This error arises from variations in the burn profile and action time of the midcourse-stage motor, the control accuracy of the nozzle positioning, and finite data rates. These inaccuracies lead to a heading error, which yields a projected ZEM error through the range-to-go to intercept,

$$1\sigma\ \mathrm{ZEM}_{\mathrm{HEC}} = \sigma_{\mathrm{HEC}} R_{\mathrm{go}}$$

For convenience the two interceptor heading error terms may be combined to produce a total heading error so that

$$\sigma_{\mathrm{HE}} = \left(\sigma_{\mathrm{HEC}}^2 + \sigma_{\mathrm{HE}N}^2\right)^{\frac{1}{2}}$$

The range-to-go may be approximated by the time-to-go to intercept and the interceptor average speed remaining

$$R_{\mathrm{go}} = V_{MR} t_g$$

The ZEM due to the interceptor guidance and control heading error at a specific time-to-go to intercept is related to the heading error by

$$1\sigma\ \mathrm{ZEM}_{\mathrm{HE}} = \sigma_{\mathrm{HE}} V_{MR} t_g$$

In this analysis, two sets of weapon system and interceptor errors will be investigated illustrating the effect of errors on 1) the optimal selection of pulse split, 2) the maximum feasible mission time, and 3) the maximum feasible intercept range. Table 2 defines the 3σ values for the two error sets for the error tree topology of Fig. 3. These might represent the errors associated with two different weapon system choices such as a surface based sensor vs a satellite system.

Earliest Burnout and Ignition Time for the Second Pulse

The requirement that the KKV must be able to steer out the 3σ ZEM measured at the end of the second-pulse burnout leads to a limit on how early the second pulse may burn out. Figure 4 shows these considerations, which set the limit for an earliest possible second-pulse ignition and burnout mission. Figure 4 gives the ZEM and the divert capabilities of the second pulse and the KKV along the vertical axis vs the flight time from the first-pulse burnout to the intercept. The ignition and burnout time of the first pulse is fixed and is fired as early as possible based on interceptor requirements. The 3σ ZEM at the second-pulse burnout (ZEM_3) decreases as the burnout (and, thus, the ignition) of the second pulse is delayed. If the second pulse burns out before the 3σ ZEM drops below the maximum divert of the KKV, then the 3σ handover conditions will exceed the capabilities of the KKV. This would be considered a failed mission design. Thus, the burnout of the second pulse must be delayed until the intersection of the second-pulse burnout 3σ ZEM and the KKV maximum divert lines. This sets the earliest time-to-go and the earliest time for the second-pulse burnout. The interceptor 3σ ZEM history for an earliest second-pulse burnout mission is shown with the dark line in the Fig. 4. The 3σ ZEM history starts at the first-pulse burnout value until ignition of the second pulse at such a time A that the second pulse burnout event B occurs at the intersection of the second-pulse burnout 3σ ZEM

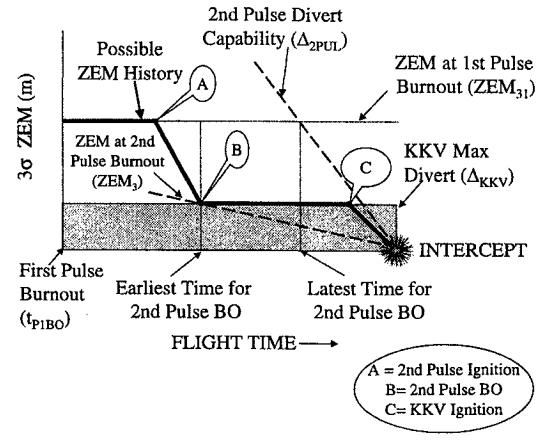

Fig. 4 Earliest firing mission 3σ ZEM history.

line and the KKV maximum divert line. The interceptor then coasts with constant 3σ ZEM from this point until ignition of the KKV at C. The KKV then drives the 3σ miss to practically zero.

The error tree model from Fig. 3 may be applied at the second-pulse burnout to determine the earliest time-to-go at which the second pulse may burn out for a successful mission. The 3σ ZEM existing at the midcourse-stage second-pulse burnout can be developed by combining the error sources assuming zero correlation through the junction operator:

$$3\sigma\ \mathrm{ZEM}_3 = 3\left(V_{MR2}^2 \sigma_{\mathrm{HE}}^2 t_{\mathrm{gmc}}^2 + \sigma_{\mathrm{VTGT}}^2 t_{\mathrm{gmc}}^2 + \sigma_{\mathrm{POS}}^2\right)^{\frac{1}{2}}$$

To ensure a high probability of intercept then the achievable divert displacement of the KKV must equal or exceed the 3σ value of the expected ZEM at midcourse-stage second-pulse burnout. That is,

$$K_{\mathrm{ge}} \Delta_{\mathrm{KKV}} \geq 3\sigma\ \mathrm{ZEM}_3$$

The greatest allowable value of the time-to-go at midcourse-stage burnout $t_{\mathrm{gmc\,max}}$ may be determined from this equation. For convenience in solution, the direct position errors will be neglected because these are usually small compared to the target velocity measurement error and the interceptor heading error contributions.

Then the equation for the earliest time-to-go for the burnout of the second pulse is

$$t_{\mathrm{gmc\,max}} = \frac{K_{\mathrm{ge}} \Delta_{\mathrm{KKV}}}{3\left(V_{MR2}^2 \sigma_{\mathrm{HE}}^2 + \sigma_{\mathrm{VTGT}}^2\right)^{\frac{1}{2}}}$$

The earliest time-to-go for burnout of the second pulse can now be evaluated numerically using the 50/50-pulse split interceptor parameters of Table 1 and the high-quality error set from Table 2. This calculation is independent of the pulse split of the midcourse-stage motor. The average speed remaining is approximated by the midcourse-stage burnout speed of Table 1. Then, the earliest time-to-go for the second pulse to burnout is

$$t_{\mathrm{gmc\ max}} \approx 92\ \mathrm{s}$$

If the system errors do not change with increasing mission time, then the earliest time for second pulse ignition $t_{2\mathrm{ignt}}$ increases linearly with mission time by the following:

$$t_{2\mathrm{ignt}} \approx t_{\mathrm{mission}} - t_{\mathrm{gmc\ max}} - t_2$$

Latest Burnout and Ignition Time for the Second Pulse

The requirement for the second pulse of the midcourse stage to correct the errors from the first-pulse burnout leads to a limit on the latest time for the second pulse to burn out. Figure 5 shows some of the considerations that set this limit for a second-pulse latest time-to-burnout mission. The value of the available second-pulse divert displacement if it burns out at the current time $\Delta_{2\mathrm{PUL}}$ decreases as the second-pulse burnout (and, thus, ignition) is delayed. As long

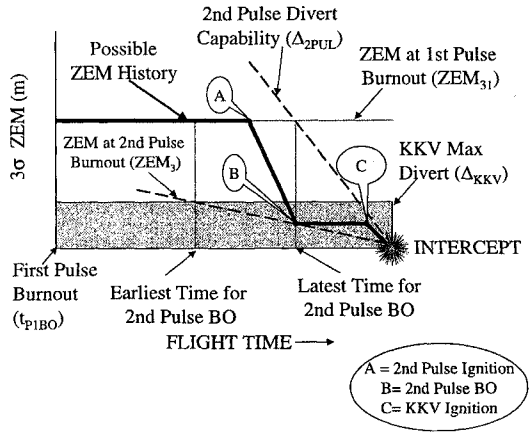

Fig. 5 Latest firing mission 3σ ZEM history.

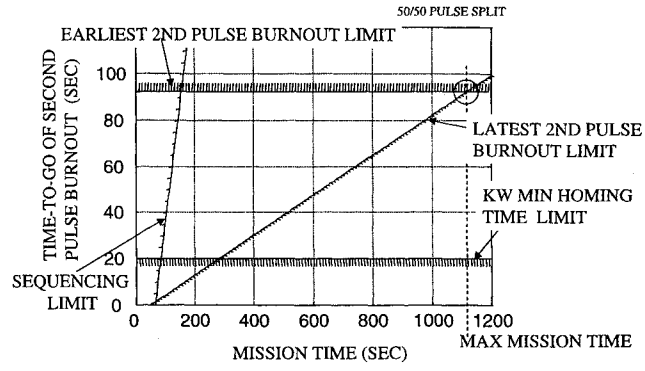

Fig. 6 Mission chart for 50/50 interceptor and high-quality errors.

as the second-pulse divert is greater than the 3σ ZEM from the first pulse, the mission design can be considered successful. For a successful mission design, the second pulse must burn out before the intersection of the second-pulse available divert line and the first-pulse burnout 3σ ZEM line. The 3σ ZEM history for a mission that uses a latest allowable second-pulse burnout time is indicated in Fig. 5 with a dark line. For this mission, the 3σ ZEM stays at the first-pulse burnout value until the second pulse is fired at A. This point represents t_2 seconds before the intersection of the second-pulse divert displacement and the first-pulse 3σ ZEM value. After second-pulse ignition, the 3σ ZEM value decreases until burnout at B. The resulting 3σ ZEM will be less than the KKV maximum divert value. The interceptor then coasts until KKV activation, which drives the 3σ miss essentially to zero at the intercept. The first-pulse burnout error tree may be used to develop a relationship for the latest time-to-go for the second pulse to burnout and the latest time for the second pulse to be ignited.

The available divert displacement of the second pulse is approximately

$$\Delta_{2PUL} = \Delta V_{2PUL} t_{gmc}$$

The divert displacement of the second pulse must be great enough to steer out the 3σ ZEM from the burnout of the first pulse. That is,

$$\Delta V_{2PUL} t_{gmc} \geq 3\sigma\ ZEM_{31}$$

Thus, the burnout time of the second pulse can occur no later than

$$t_{gmc\ min} = \frac{3\sigma\ ZEM_{31}}{\Delta V_{2PUL}}$$

The ZEM can be estimated by combining the elements of the error tree for the first pulse burnout. Then the total first-pulse burnout 3σ ZEM (neglecting the direct position error) is given by

$$3\sigma\ ZEM_{31} \approx 3\left(\sigma_{HE}^2 V_{MR1}^2 t_{g1bo}^2 + \sigma_{VTGT}^2 t_{g1bo}^2\right)^{\frac{1}{2}}$$

The time-to-go at the first pulse burnout is $t_{g1bo} = t_{mission} - t_{p1bo}$. Then for a successful intercept, the second pulse must burn out at a time-to-go no later than

$$t_{gmc\ min} \approx 3\frac{\left(\sigma_{HE}^2 V_{MR1}^2 + \sigma_{VTGT}^2\right)^{\frac{1}{2}} (t_{mission} - t_{p1bo})}{\Delta V_{2PUL}}$$

As the mission time increases, ZEM_{31} increases and the second pulse burnout must occur at earlier time-to-go values. A numerical evaluation of the latest time-to-go limit for the interceptor with the 50/50-pulse split can now be presented. The interceptor parameters from Table 1 are used with the average remaining speed approximated by the first-pulse burnout speed. Therefore, for the high-quality error set from Table 2, the second pulse must burn out at a time-to-go no later than

$$t_{gmc\ min} = 0.085(t_{mission} - t_{p1bo})$$

Then the latest time to ignite the second pulse is given by

$$t_{2ignt} \approx t_{mission} - t_{gmc\ min} - t_2$$

Second-Pulse Burnout Window and the Mission Chart

The earliest and latest time-to-go constraints for the second-pulse burnout create both a burnout and a firing window for the second-pulse. The burnout window may be combined graphically with several constraints on the mission timelines to create the concept of the mission chart. The first step in creation of the mission chart is to numerically evaluate the second-pulse burnout constraints. In this analysis, the interceptor parameters from Table 1 are used. To preserve the insight provided into a relatively complex phenomenon, some discretion is required in selecting the values for the calculation. Most notably, this caveat applies to the selection of the average speed remaining values. The average speed remaining after first-pulse burnout is approximated by the peak burnout speed at first-pulse burnout for each configuration. This has the effect of underestimating the average speed remaining for short-range intercepts and overestimating it for the long-range intercepts. Because the mission chart concept attempts to coalesce all intercepts to a single chart, this averaging effect is desirable. The average speed remaining after second-pulse burnout is approximated by the peak burnout speed after second-pulse burnout for each configuration as given in Table 1. Additionally, steady-state values of the system errors averaged over the entire intercept space are typically used for estimating the burnout limits such as those presented in Table 2.

The resulting second-pulse burnout window is shown in Fig. 6 for the 50/50-pulse split interceptor and for the high-quality error set. The mission chart is defined in terms of the time-to-go to intercept at second-pulse burnout, t_{gmc}, and the mission time, which is defined as total flight time to the intercept. The earliest and latest time-go-burnout limits are shown on the chart. In developing the mission chart, the intersection of these two constraints provides one measure of the maximum mission time possible, which is the point that there is a zero width window. This is shown with a circle in Fig. 6. Intercepts requiring flight times longer than the value associated with this intersection would be infeasible. This limit on mission time is defined as the error derived mission time limit. Also shown on the mission chart is an additional constraint on the feasible space, which is the sequencing limit. This constraint places another earliest time-to-go limit on the second-pulse burnout such that second-pulse ignition occurs after first-pulse burnout. This has the effect of limiting the burnout and firing window for short missions.

Kinematic Limit

The error derived mission time from the mission chart represents one measure of the maximum possible mission time. Another important limit to be applied to the mission chart is the maximum useful flight time based on the interceptor kinematics. Under the assumption that the minimum flight time trajectory to an intercept point shall always be the preferred solution, the maximum useful flight time is the time to the maximum range. In the absence of weapon system detection limits, the maximum range of the interceptor and

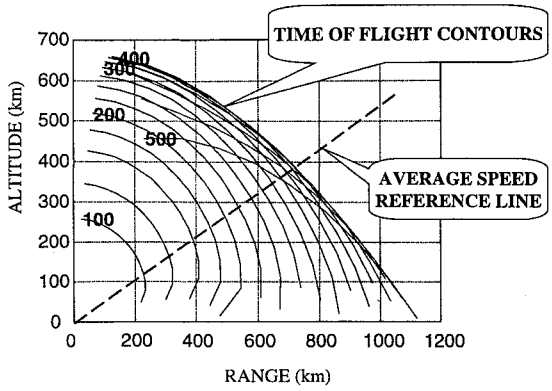

Fig. 7 Flight time contours for 50/50 interceptor.

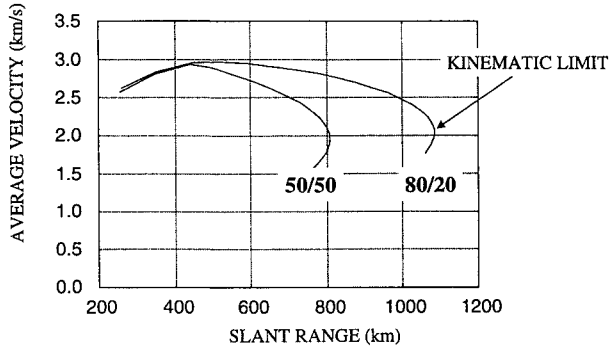

Fig. 8 Average speed for two pulse splits.

the corresponding flight time is a function of 1) the altitude of the intercept, 2) the maximum burnout speed of the interceptor, 3) the pulse split, and 4) the time-to-go at which the second pulse is fired. To increase the kinematic reach of the interceptor, it is best to fire the second pulse as early as possible. Because the KKV divert and the system error sources dictate the earliest the time-to-go to fire the second pulse, these indirectly affect the maximum useful flight time. To address the altitude dependence, the maximum mission time or kinematic limit is defined as the flight time for a maximum range mission along a 30-deg slant from the launch point in local altitude and surface range space. This slant angle is felt to represent the majority of the intercept population. As the kinematic limit is reached, the time-of-flight contours begin to coalesce.

The kinematic limit is shown in Fig. 7, which presents the time-of-flight contours for the interceptor with the high-quality error set, 50/50-pulse split, and for the second pulse fired as early as possible at 92-s time-to-go. The time-of-flight contours are generated assuming zero error corrections. The kinematic limit for this case is 425 s, which is taken as the longest useful flight.

The effect of pulse split on the kinematic limit is shown in Fig. 8, which shows the average speed for the high-quality error set and the 50/50-pulse interceptor and the 80/20-pulse interceptor along the range–altitude reference line in Fig. 7. For both pulse splits, the second pulse is fired at the earliest possible time. The kinematic limit is indicated and is the time of flight where the average speed begins to sharply decline. The reduction in average speed between the 80/20 split and the 50/50 split is clearly shown.

The quality of the system errors has an indirect effect on the average speed along the range-altitude reference line. The low-quality error set requires that the second pulse burn out later than the high-quality error set leading to lower average speeds when the second pulse is fired as early as possible.

If the second pulse is fired at a later time-to-go than in the previous example, then the average speed of the missile and kinematic limit are reduced. Thus, the kinematic limit is a function of the time-to-go at the second-pulse burnout. The mission charts can include this effect but the difference in the kinematic limit over the range of second-pulse burnout time-to-go values in these mission charts is within the precision of the determination of the kinematic limit.

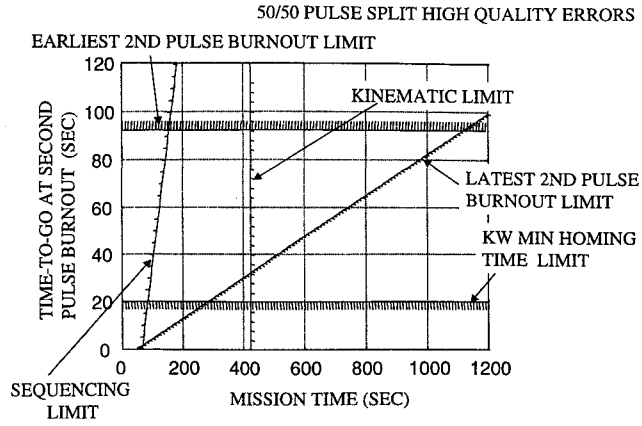

Fig. 9 Mission chart with kinematic limit.

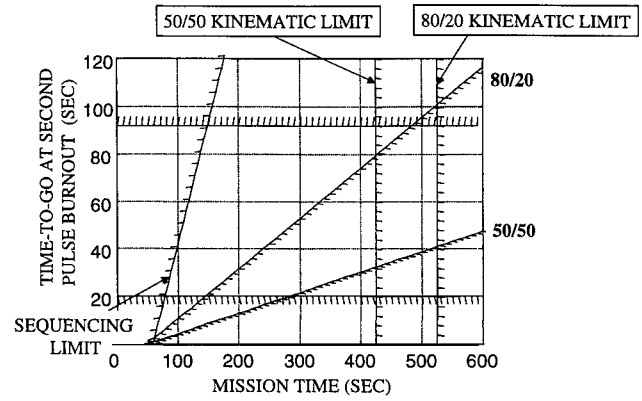

Fig. 10 Mission chart with high-quality errors for two pulse splits.

Balancing the System with Mission Charts

The kinematic limit completes the mission chart and allows it to be used to determine the pulse split that maximizes the system performance by bringing the kinematic and error derived mission time limits into balance. The kinematic limit can be superimposed on the earlier mission charts to demonstrate the reduced feasible region. Figure 9 shows the mission chart from Fig. 6 with the kinematic limit superimposed. The kinematic limit is the more restrictive limit and, thus, it sets the maximum feasible mission time.

Figure 10 shows the mission charts for the 50/50 and 80/20 missiles using the high-quality error set. The kinematic limit is increased for the 80/20 missile to 525 s, whereas the 50/50 interceptor only has a 425-s kinematic limit. For the 80/20 missile the maximum mission is now set by the error derived mission time limit. The error derived mission time limit and the kinematic limit for the 80/20 interceptor are approximately equal. Thus, the 80/20 system can be considered balanced for the high-quality error set. The 50/50-interceptor system is unbalanced because the error derived mission time limit is much greater than the kinematic limit. The divert capabilities of the 50/50 midcourse-stage rocket motor and the KKV are much greater than required for the high-quality error set. In addition, the average speed for the 80/20 interceptor will be higher than the 50/50 interceptor to the longer range intercepts. Thus, for the high-quality error set, the 80/20 interceptor produces a superior system by maximizing the average speed and the maximum feasible mission time. This will lead to an increase in the defended reach of the system.

Figure 11 shows the mission chart for the 50/50 and the 80/20 interceptors with the low-quality error set. The higher system errors shift the latest and earliest time-to-go at burnout lines so as to reduce the second-pulse burnout and firing windows for any specific mission time as compared to the high-quality error set. The 80/20 interceptor has a very limited maximum feasible mission time of 190 s set by the error derived mission time limit. The full kinematic limit of 525 s for the 80/20 interceptor cannot be used. Whereas the maximum mission of the 50/50 missile is also set by the error derived mission time limit of 400 s, this equals the kinematic limit.

Table 3 Defensive reach results

Error set	Pulse split	Maximum mission time, s	Maximum feasible intercept range, km
High quality	50/50	425	960
High quality	80/20	475	1300
Low quality	50/50	400	880
Low quality	80/20	190	510

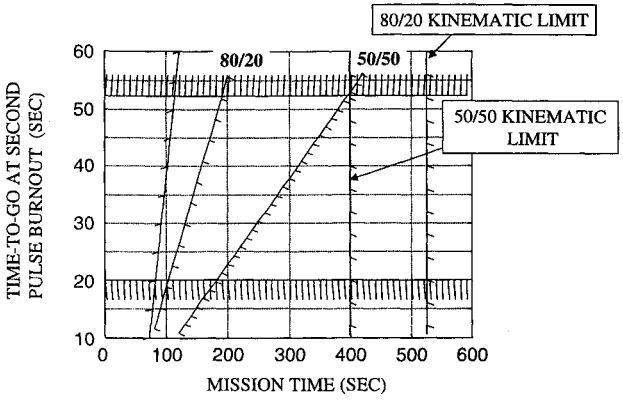

Fig. 11 Mission chart with low-quality errors for two pulse splits.

Thus, the 50/50 missile is in balance with the expected system errors. For the low-quality error set the 50/50 split is the preferred option.

The mission charts have concentrated on the mission times and have demonstrated the improvements in maximum mission time possible by the appropriate selection of the pulse split. The maximum mission time and the average speed to this point will determine the maximum feasible intercept range (in the absence of detection range limits). For missions where an interpulse delay is required, the 80/20 interceptor has the greater average speed. Table 3 shows the maximum intercept range at 150-km altitude for the considered pulse splits and error sets. Proper selection of the pulse split, e.g., the 50/50, for the low-quality error set increases the maximum feasible intercept range by 70%. For the high-quality error set, use of the 80/20 increases the maximum intercept range by 33% as compared to the 50/50 interceptor.

Conclusions

Generally, the second pulse should be fired as early as possible subject to the earliest midcourse-stage burnout time-to-go limit so as to maximize the average speed. If the midcourse-stage second-pulse ignition must be delayed so as to accommodate a mission event such as weapon system discrimination of the threat complex, then it should occur early enough so that the burnout occurs before the latest burnout time-to-go to intercept limit.

For the high-quality error set, the maximum mission time and maximum feasible intercept range increase significantly as the fraction of propellant in the first pulse increases. Thus, for this error set the 80/20 split would be preferred largely because of its ability to increase the average speed and the maximum feasible intercept range. For the low-quality error set, the collapsing of the second-pulse burnout window at the error derived mission time limit determines the maximum feasible mission time. The use of the 50/50-pulse split extends this intersection out to the kinematic limit. Thus, for the low-quality error set, the 50/50 split balances the system and increases the maximum feasible intercept range by 70%.

The optimal allocation of the pulse split is a function of the expected system errors and the divert capability of the KKV. A lower quality system will tend to require smaller initial fractions with highly accurate systems favoring larger initial propellant fractions.

In the absence of detection range limits, the total system errors are a significant factor in determining the maximum feasible intercept range.

Acknowledgments

The Associate Editor, Stephen Osder, and the reviewers provided many useful comments to clarify the key points of this paper and to relate this analysis to the larger issues of exoatmospheric interceptor design. Ernest Ohlmeyer of the U.S. Naval Surface Warfare Center, Dahlgren Division (NSWCDD), provided many significant insights into the error phenomenology. In addition, individuals from many organizations have contributed to the development of the error tree concept. Michael Libeau of NSWCDD provided significant contributions to this paper. The continued support of George Long of NSWCDD made this work possible.

References

[1]Calise, A. J., and Nagy, J., "Necessary Conditions for Optimal Pulse Control," AIAA Paper 85-1955, Aug. 1985.

[2]Calise, A. J., and Prasad, J. V. R., "Pulse Motor Control for Maximizing Average Velocity," *Journal of Guidance, Control, and Dynamics*, Vol. 12, No. 2, 1989, pp. 169–174.

[3]Wassom, S. R., and Gunderson, R. W., "Optimal Pulse Motor Control," AIAA Paper 89-0383, Jan. 1989.

[4]Cheng, V. J. L., Menon, P. K. A., Gupta, N. K., and Briggs, M. M., "Reduced Order Pulse Motor Ignition Logic," *Journal of Guidance, Control, and Dynamics*, Vol. 10, No. 4, 1987, pp. 343–350.

[5]Mennon, P. K. A., Cheng, V. H. L., Lin, C. A., and Briggs, M. M., "High Performance Missile Synthesis with Trajectory and Propulsion System Optimization," *Journal of Spacecraft and Rockets*, Vol. 24, No. 6, 1987, pp. 552–557.

[6]Phillips, C. A., "Energy Management for Multiple Pulse Missiles," *Journal of Spacecraft and Rockets*, Vol. 27, No. 6, 1990, pp. 623–629.

[7]Imado, F., Kwoda, T., and Susumu. M., "Optimal Thrust Control of a Missile with a Pulse Motor," *Journal of Guidance, Control, and Dynamics*, Vol. 14, No. 2, 1991, pp. 377–382.

[8]Ohlmeyer, E. J., Pepitone, T. R., Miller, B. L., Malyevac, D. S., Bibel, J. E., and Evans, A. G., "GPS-Aided Navigation Systems Requirements for Smart Munitions and Guided Missiles," AIAA Paper 97-3683, Aug. 1997.